Validation of GOCE Simulation[1]

J. Müller, H. Oberndorfer

Institute for Astronomical and Physical Geodesy (IAPG), Technische Universität München
D-80290 München, Germany (email: jxmx@bv.tum.de)

Abstract

The gradiometer mission GOCE (Gravity Field and Steady-State Ocean Circulation Explorer) is simulated by using simplified assumptions. Taking into account the couplings between the different sensors (e.g. GPS, accelerometers) and control systems (e.g for drag-free control), we investigate the effects of different error sources on the scientific end-products like gravity gradients (or spherical harmonics at a further processing level).
We try to simulate the total mission (i.e. considering all important effects from misalignment of gradiometer axes up to instabilities of the contol loops) by using the standard mathematical software package SIMULINK.
We control our simulation results by linear control theory; that means, we extract single parts of the complex mission (e.g. drag-free control or the coupling of misalignments) and compute their effects separately.
Although the possibilities of SIMULINK are limited good results have been obtained. Our preliminary results show that the aspired accuracy level for GOCE (10^{-3} Eötvös/$\sqrt{\text{Hz}}$) can be achieved which enables to derive a gravity field up to degree and order 250.

1 Introduction

GOCE is one of the dedicated gravity field mission currently under investigation in the context of the ESA explorer program. Its main objective is the determination of the Earth's gravity field with high spatial resolution and with high homogeneous accuracy by using: Satellite-to-Satellite Tracking (SST) in high-low mode for the orbit determination and for the retrieval of the long-wavelength part of the gravity field, and Satellite Gravity Gradiometry (SGG) for the derivation of the medium/short-wavelength parts.
The GOCE orbit will be near circular and sun-synchronous ($i \approx 97^o$) at an altitude of 250 km. The mission duration is planned to be about 8 months. During this period the satellite shall be kept drag-free. The orbit will be determined by GPS with an accuracy of about 1 cm RMS. The measurement precision of the 3-axis gradiometer that is aimed for, is at the 10^{-3} Eötvös/$\sqrt{\text{Hz}}$ level.
Beside a GPS receiver and an ensemble of 3-axis accelerometers, further instruments are needed; e.g. star trackers to determine the orientation of the spacecraft or thrusters for attitude and drag-free control. Each instrument has its own error behaviour which affects the measurements and the final products in some typical manner.
For a realistic simulation, the various errors (e.g. misalignments, drag coupling or S/C rotation) as well as the interactions between the sensors/actuators (e.g. for attitude control) have to be considered and their effect on the scientific end-products (e.g. spherical harmonics, geoid heights or gravity anomalies) has to be investigated.
The different parts of the GOCE simulation are performed by the SID consortium consisting of SRON[2], IAPG and DEOS[3]. The division of the different tasks within SID is shown in Fig. 1. Additionally, IAPG is responsible for the validation of the gradiometer simulation.

[1] This article is published in similar form in the journal *Artificial Satellites*.
[2] Space Research Organisation Netherlands, NL-3584 CA Utrecht, NL.
[3] Delft Institute for Earth Oriented Space Research, Delft University of Technology, NL-2629 JA Delft, NL.

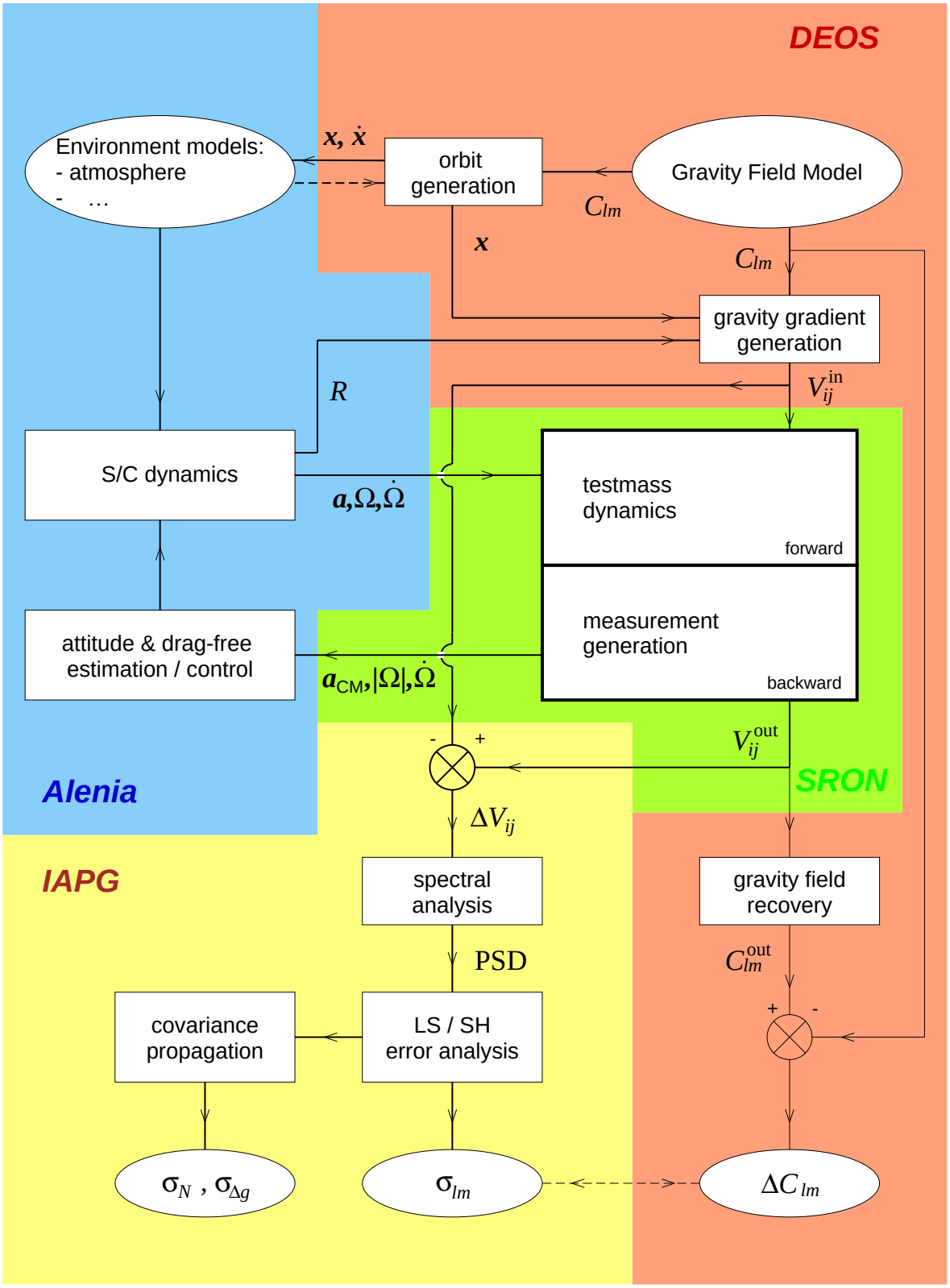

Figure 1: Simulation of GOCE by SID.

The global simulation of the gradiometer measurements is performed by SRON (see Hoyng, 1997) with input from DEOS and ALENIA[4]. Our (IAPG) goal is the validation of the results of the GOCE simulator by using simplified assumptions. For this purpose, we use two different techniques: first, we extract single parts of the complex mission (e.g. drag-free control or the coupling of misalignments) and compute their effects by linear control theory; secondly, we simulate the total mission by using the mathematical software package SIMULINK. There the measurement principles and the relation between the various instruments are represented by means of a flow chart which is also the computer program itself in SIMULINK.

2 Basic Equations

The basic equation of gradiometric measurements is given by (e.g. Rummel, 1986)

$$\mathbf{\Gamma} = \mathbf{V} + \mathbf{\Omega\Omega} + \dot{\mathbf{\Omega}}. \tag{1}$$

$\mathbf{\Gamma}$ represents the tensor of the observables and $\mathbf{V}$ describes the second derivatives of the gravitational potential of the Earth. It reads

$$\mathbf{V} = \begin{pmatrix} V_{xx} & V_{xy} & V_{xz} \\ V_{yx} & V_{yy} & V_{yz} \\ V_{zx} & V_{zy} & V_{zz} \end{pmatrix}. \tag{2}$$

The tensor is symmetric und trace-free, i.e. in each point along the orbit 5 of its 9 elements are linearly independent.
Here we adopt a coordinate frame which is co-moving with the satellite, x points in flight direction (along-track), y is orthonormal to the orbit plane (cross-track) and z is the radial component[5].
$\mathbf{\Omega\Omega}$ and $\dot{\mathbf{\Omega}}$ describe the effect of the inertial forces on the observations (where a Coriolis-like term has been neglected because the test masses of the accelerometers almost don't move). They are computed from the angular velocities $\mathbf{\Omega}$ resp. their time derivatives (indicated by the dot over the variable).

$$\mathbf{\Omega\Omega} = \begin{pmatrix} -\Omega_y^2 - \Omega_z^2 & \Omega_x\Omega_y & \Omega_x\Omega_z \\ & -\Omega_x^2 - \Omega_z^2 & \Omega_y\Omega_z \\ \text{symm.} & & -\Omega_x^2 - \Omega_y^2 \end{pmatrix}, \tag{3}$$

$$\dot{\mathbf{\Omega}} = \begin{pmatrix} 0 & \dot{\Omega}_z & -\dot{\Omega}_y \\ -\dot{\Omega}_z & 0 & \dot{\Omega}_x \\ \dot{\Omega}_y & -\dot{\Omega}_x & 0 \end{pmatrix}. \tag{4}$$

The latter matrix is anti-symmetric, whereas the former one is symmetric.

The key payload for GOCE is the gradiometer. It consists of a combination of six 3-axis accelerometers. The accelerometers are arranged in the so-called diamond configuration (see Fig. 2) which means the accelerometers are placed at six locations symetrically about the origin **G** of the gradiometer at a distance of about 25 cm from **G**. The sensitive axes of the accelerometers are oriented along the axes of an orthogonal triad. In case of the capacitive ONERA[6] accelerometer one axis is less sensitive

[4]The Italian Space Organisation ALENIA Aerospazio - Space Division is the main contractor of ESA for the study phase A of GOCE.

[5]In the case of a non-circular orbit, y remains cross-track, z points radially to the geocenter and x completes the frame to an orthonormal basis; then x is directed not longer exactly along-track.

[6]Office National d'Etudes et de Recherches Aerospatiales.

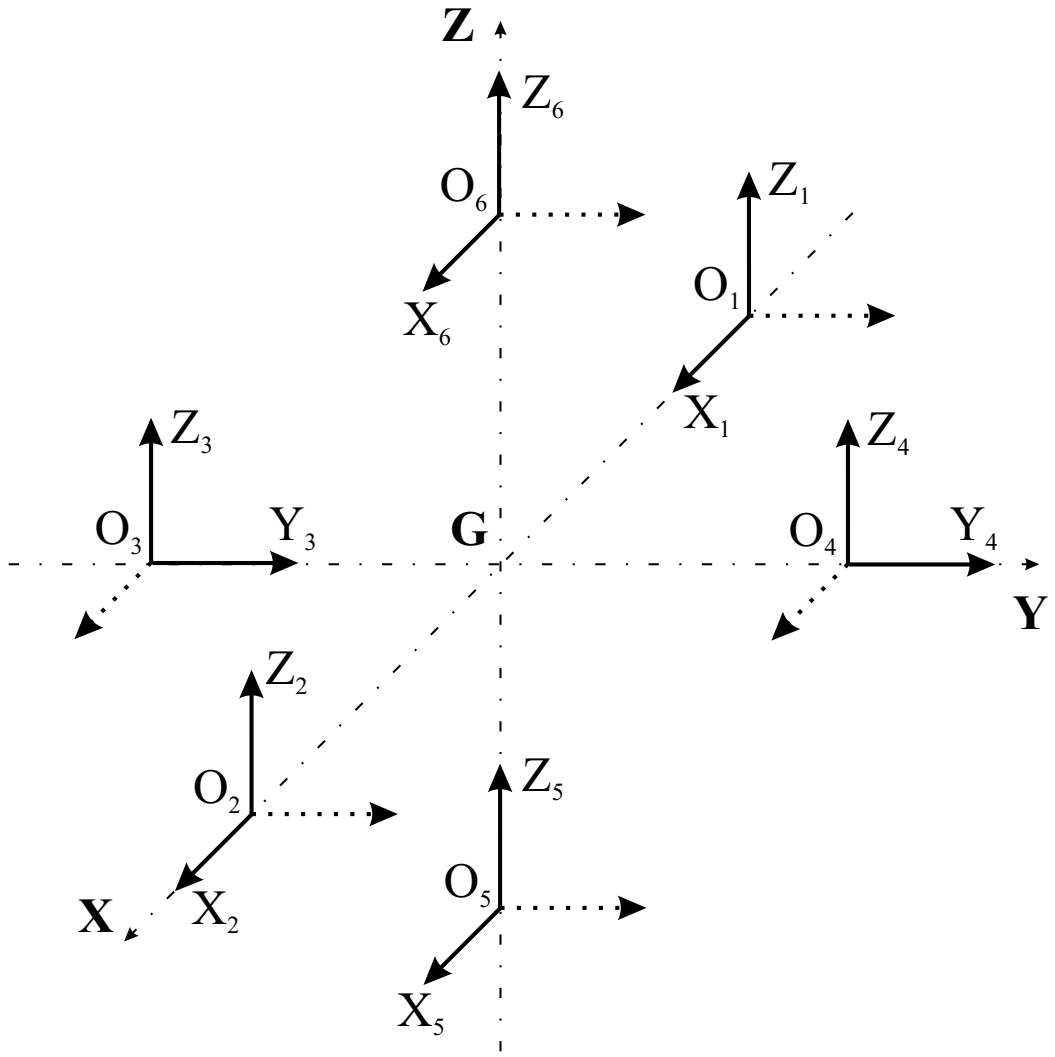

Figure 2: Diamond configuration.

than the two others. This is indicated by the dotted lines. The orientation of the sensitive axes shown in Fig. 2 is one possible option for GOCE. The two highly sensitive axes are oriented in such a way that one is able to measure the diagonal components of the gravitational tensor as well as the Γ_{xz} and Γ_{zx} components with highest accuracy. The latter is necessary to be able to solve for the angular acceleration $\dot{\Omega}_y$ (resp. the angular velocity Ω_y after time integration) which is obtained by the combination of these two off-diagonals (see Eq. (4)). If choosing another orientation of the sensitive axes, Ω_y has to be determined by another method, e.g. by using the trace of the measurement tensor. $\mathbf{\Omega}$ gives the rotation of the earth-pointing, satellite-fixed coordinate frame with respect to an inertial frame. The rotation about the cross-track axis Ω_y has to be determined with highest accuracy because it is the largest angular velocity which can be seen from (here $\mathbf{\Omega}$ represents a vector)

$$\mathbf{\Omega} = \begin{pmatrix} \delta\Omega_x \\ \Omega_y^0 + \delta\Omega_y \\ \delta\Omega_z \end{pmatrix} \tag{5}$$

where Ω_y^0 is given by the mean motion of the satellite. Therefore Ω_y produces the largest effects in the corresponding error terms.

The basic equation of gradiometric measurements (1) can also be understood as the measurement of differential accelerations over short baselines. For example the component Γ_{xx} can be obtained by

$$\Gamma_{xx} = \frac{a_1^x - a_2^x}{l} \tag{6}$$

where a_1^x and a_2^x are the accelerations along the x-axis observed with accelerometer 1 and 2, l is the distance between both accelerometers, i.e. the distance O_1O_2.
Starting from this point of view one can simulate the gradiometric observations as a combination of acceleration measurements. The acceleration in a rotating frame at a position $\mathbf{r}$ is given by

$$\ddot{\mathbf{r}} = \mathbf{F} + (\mathbf{V} + \boldsymbol{\Omega}\boldsymbol{\Omega} + \dot{\boldsymbol{\Omega}})\,\mathbf{r}. \tag{7}$$

$\mathbf{F}$ stands for the sum over all non-gravitational accelerations, mainly caused by air drag and thruster firing.
In the simulation, one can additionally assume that the position is not known perfectly

$$\mathbf{r} = \mathbf{r_0} + \delta\mathbf{r}. \tag{8}$$

That means, the distance $\mathbf{G}O$ is known up to a certain accuracy level only (e.g. 50 μm).
The angular velocity $\boldsymbol{\Omega}$ is a function of the satellite rotational dynamics (see e.g. Kaplan, 1976; Schneider, 1992). The (kinematic) Eulerian equations read

$$\boldsymbol{\Omega} = \dot{\mathbf{R}}\mathbf{R}^t \tag{9}$$

where $\mathbf{R} = D_1(\psi_x)D_2(\psi_y)D_3(\psi_z)$ is the rotation matrix calculated by 3 rotations about 3 angles, $\dot{\mathbf{R}}$ its time derivative. Eq. (9) describes the relationship between the angular velocities $\boldsymbol{\Omega}$ and the time derivatives of the angles. In detail one has

$$\begin{aligned}
\Omega_x &= \dot{\psi}_x - \dot{\psi}_z \sin\psi_y, \\
\Omega_y &= \dot{\psi}_z \sin\psi_x \cos\psi_y + \dot{\psi}_y \cos\psi_x, \\
\Omega_z &= \dot{\psi}_z \cos\psi_x \cos\psi_y - \dot{\psi}_y \sin\psi_x.
\end{aligned} \tag{10}$$

The angular accelerations can be computed by

$$\begin{aligned}
\dot{\Omega}_x &= M_x/I_x - \alpha\Omega_y\Omega_z, \\
\dot{\Omega}_y &= M_y/I_y - \beta\Omega_x\Omega_z, \\
\dot{\Omega}_z &= M_z/I_z - \gamma\Omega_x\Omega_y.
\end{aligned} \tag{11}$$

$\mathbf{M}$ are the atmospheric torques (provided by ALENIA) and $\mathbf{I}$ the principal moments of inertia defined in the satellite-fixed frame; α, β and γ are the oblateness parameters to be calculated from the moments of inertia of the S/C.

It is also appropriate to assume that the orientation of the single accelerometer axes are not perfect, i.e.

$$\ddot{\mathbf{r}}^* = \mathbf{D}\,\ddot{\mathbf{r}} \tag{12}$$

where the transformation matrix $\mathbf{D}$ is a function of misalignments, couplings of accelerometer axes, scale factors and so on.

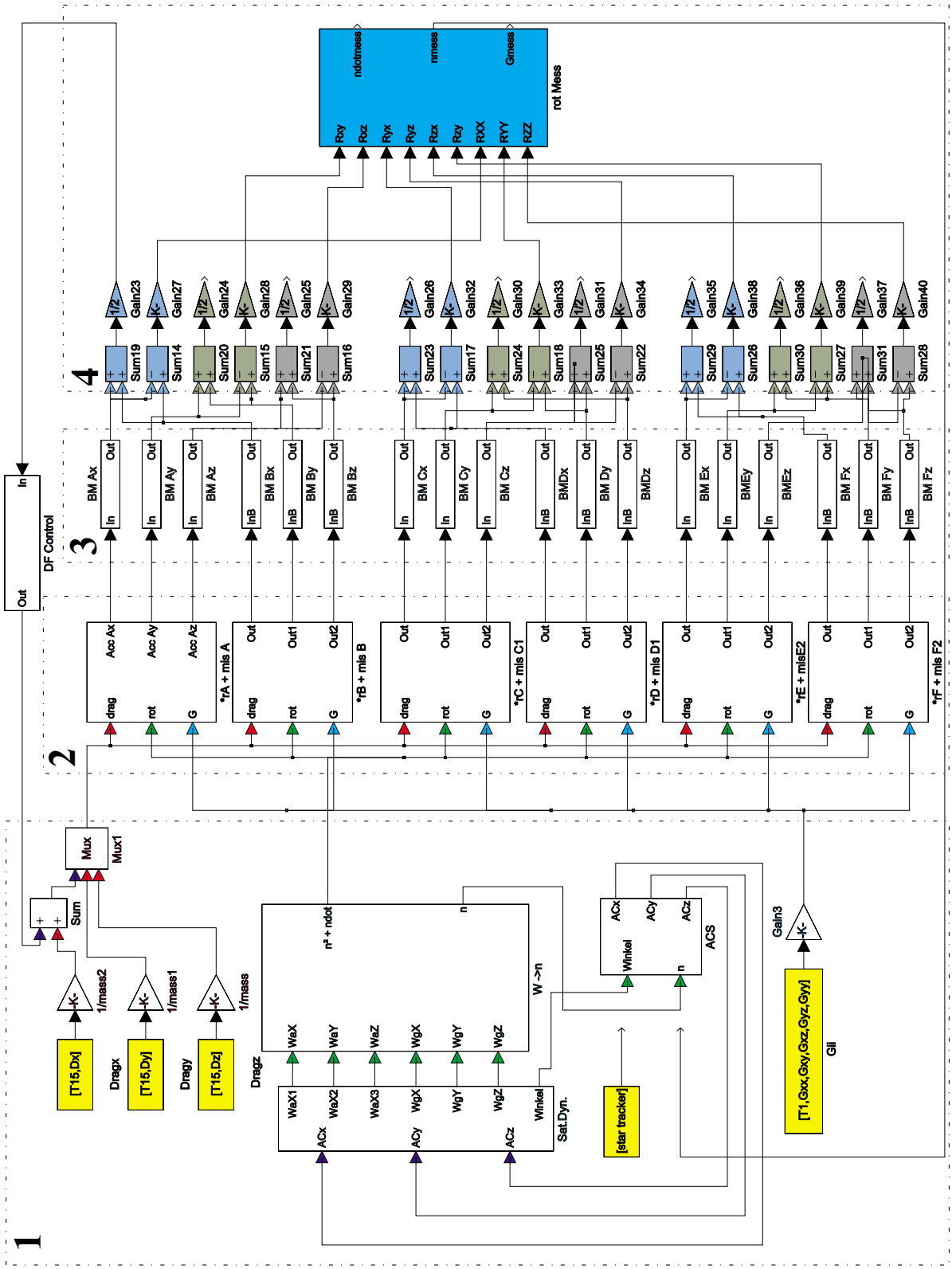

Figure 3: Validation simulator in SIMULINK.

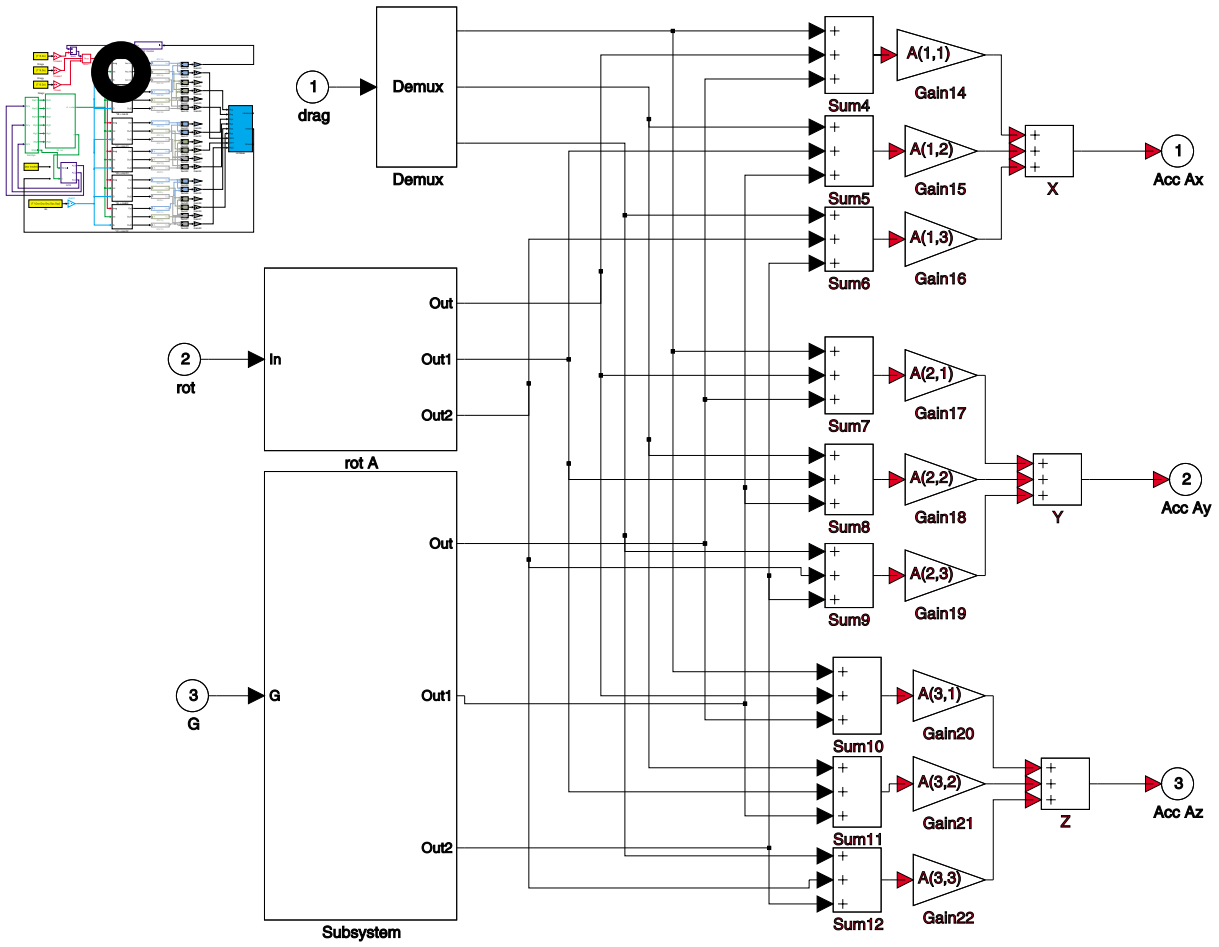

Figure 4: Computation of 'real' accelerations.

Having computed quasi-real accelerations at selected locations of the diamond configuration, the simulation of the measurement process can begin.
Using the capacitive ONERA accelerometers, the test mass is a cube in an electrical field within a housing. When the satellite (and the housing which is mounted on it) is affected by external non-gravitational accelerations the test mass tends to move, but is constrained to stay at rest ('approximately') by electrical feedback forces.
In the frequency domain, the relationship between the measured quantity, a voltage $Vo(s)$, and the external input acceleration $a_{ext}(s)$ is given by

$$\frac{Vo(s)}{a_{ext}(s)} = \frac{H(s)}{s^2 - \omega_p^2 + H(s)}, \tag{13}$$

with $-\omega_p^2 \approx -0.01$ (rad/s)^2 defines the negative parasitic stiffness and $H(s)$ the corresponding transfer function of the feed back controller

$$H(s) = \omega_0^2 \left(1 + \frac{s}{\omega_D} + \frac{\omega_i}{s}\right) \tag{14}$$

where $\omega_0 = 2\pi f_0$ ($f_0 = 5$ Hz) is the basic frequency of the accelerometer, $\omega_D = \omega_0/3$ the damping frequency and $\omega_i = \omega_0/10$ the integration frequency.

Additionally internal and external noise affect the accelerometer measurements. The resulting voltage is then again transformed into a 'measured' acceleration.

The combination of the readouts of the six accelerometers and (anti-)symmetrisation gives on the one hand

$$\dot{\mathbf{\Omega}} = \frac{1}{2}(\mathbf{\Gamma} - \mathbf{\Gamma}^t) \tag{15}$$

where the integration leads to $\mathbf{\Omega}$ which is then used to determine on the other hand the pure gravitational part

$$\mathbf{V} = \frac{1}{2}(\mathbf{\Gamma} + \mathbf{\Gamma}^t) - \mathbf{\Omega}\mathbf{\Omega}. \tag{16}$$

$\mathbf{\Omega}$ is used further in closed loop for attitude control (AC).
The common acceleration of two arbitrary accelerometers

$$\mathbf{F} = \frac{\ddot{\mathbf{r}}_\mathbf{2} + \ddot{\mathbf{r}}_\mathbf{1}}{2} \tag{17}$$

is a direct measure of the linear (non-gravitational) acceleration of the S/C and is used in a further control loop for drag-free control (DFC).

3 Coding with SIMULINK

SIMULINK is software where the coding is performed by constructing a flow chart, i.e. defining blocks and connecting them. The blocks itself may consist of computer programs, the connections describe mathematical functions (e.g. summation, but also numerical integration).

The structure of the main part of our GOCE simulator - the validation simulator - is shown in Fig. 3. Here, the formulas given in the previous section are translated in SIMULINK language. One can divide the simulation process in four steps indicated by the dotted frames 1, 2, 3 and 4. In frame 1 the input quantities are provided, in 2 the simulated accelerations are computed, in 3 measured accelerations are simulated and in 4 the various output quantities are computed.
The grey blocks in frame 1 describe the input quantities: linear non-gravitational forces from air drag, gravity gradients and possible star tracker observations (not yet implemented). The drag forces are transformed into linear accelerations ($\mathbf{F}$ in Eq. (7)). As seen in Eq. (7), also angular velocities and accelerations are needed. They are obtained by solving the Eulerian equations which are realised by the large block in the middle of frame 1.
Now moving from the left to frame 2 one has six large blocks. They stand for the six accelerometers of the diamond configuration (see Fig. 2). In each of these blocks, Eq. (7) is calculated for each accelerometer location (a more detailed description follows below in Fig. 4). The transformation $\mathbf{D}$ (Eq. (12)) is indicated by the short formula (e.g. 'rA + misA') just below each block. The result of these computations are 'real' accelerations at a certain position in a certain direction (x, y or z).
Moving on to frame 3 one finds 18 accelerometer axes (3 axes at 6 locations) simulating the measurement process which will be explained in detail below (see Fig. 5). The output is 'measured' accelerations.
In frame 4, they are now combined to derive common mode accelerations which are needed for DFC as well as differential mode accelerations (like Eq. (6)). For DFC, the loop is closed on the top of Fig. 3, where the measured accelerations are used to activate some proportional thrusters for drag-free control in the desired frequency bandwidth (e.g. $5{\cdot}10^{-3}$ – $7{\cdot}10^{-2}$ Hz). The differential accelerations of two measurements have to be divided by their baseline which results in a specific component of the tensor $\mathbf{\Gamma}$ which is indicated by the large block on the right hand side of frame 4.

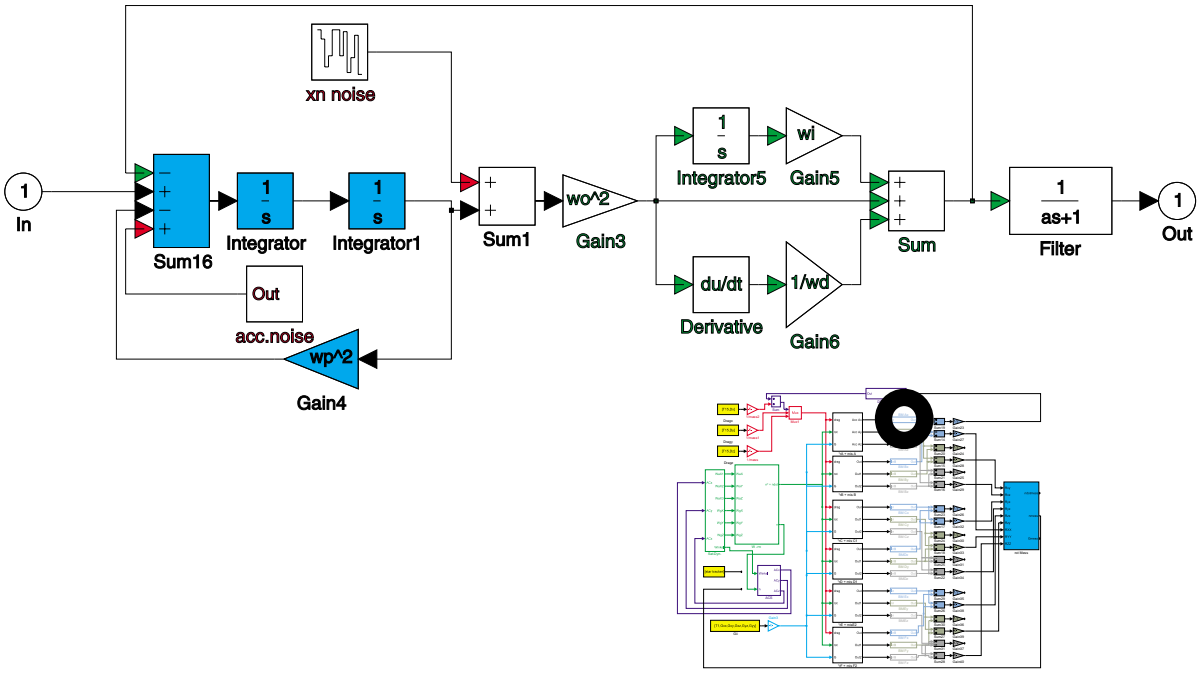

Figure 5: Capacitive Accelerometer.

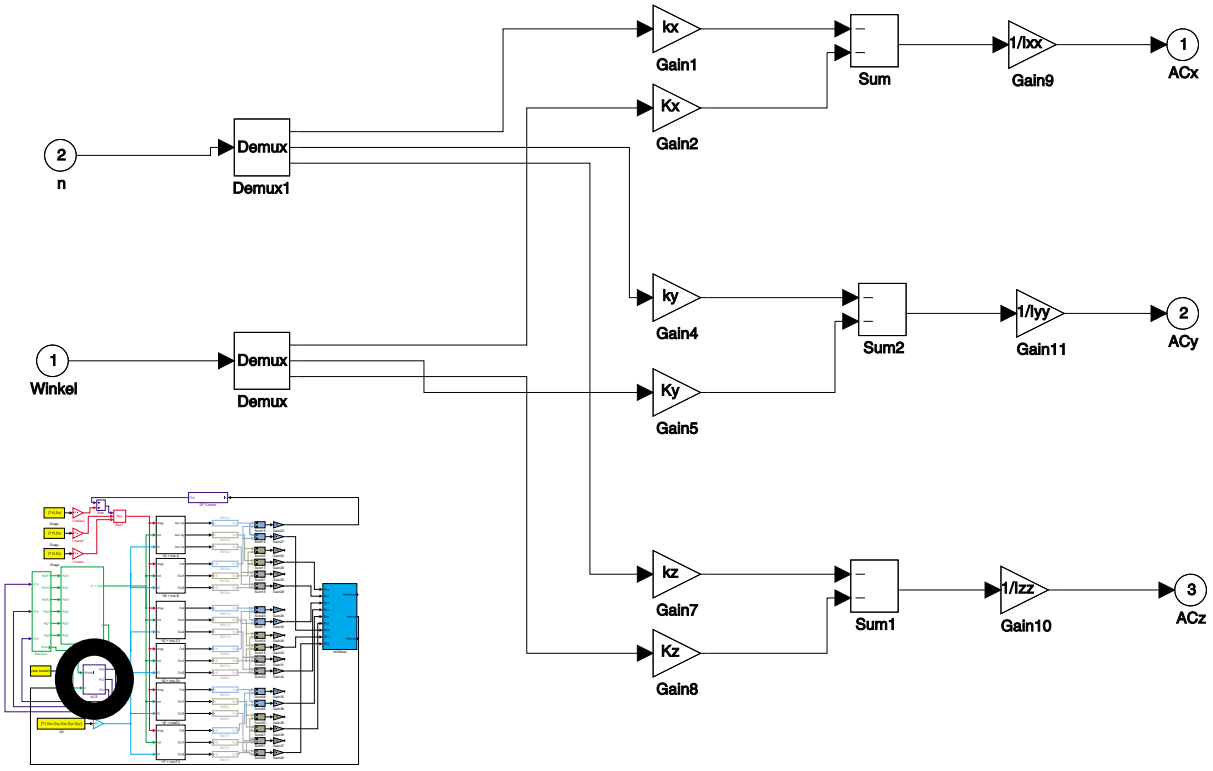

Figure 6: Attitude Control System.

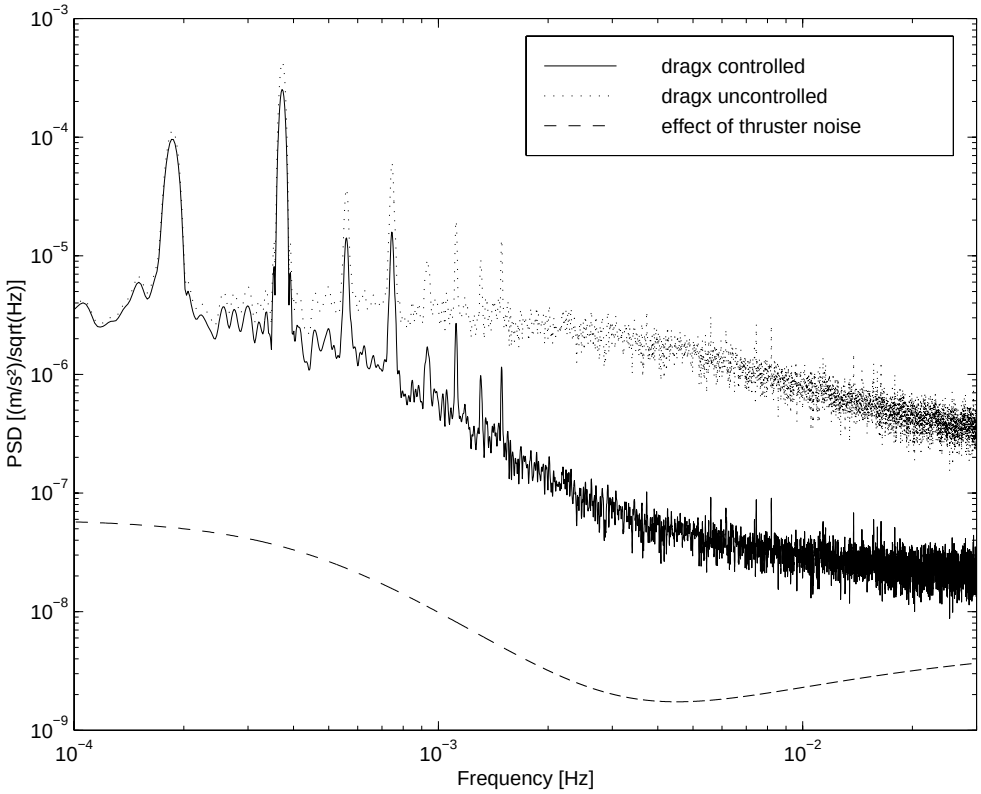

Figure 7: Test of the DFC.

(Anti-)symmetrisation allows to decouple rotational and gravitational parts of the tensor (see Eqs. (15) and (16)). The rotational parts (angular velocities) are used again in the ACS (the latter loop is not yet closed, only indicated at the bottom of Fig. 3). But the ACS is simulated with input quantities from the computation of the Eulerian equations. The ACS block is located at the lower left side of Fig. 3. It is discussed more detailed below in Fig. 6.

Fig. 4 explains the computation of Eq. (7). On the left, the input quantities enter and are multiplied by $\mathbf{r} = (x,\ y,\ z)^t$ and summed up 'line-wise'. Then the transformation $\mathbf{D}$ (in Fig. 4, the matrix components are designed by A(1,1), ...) describing misalignments, couplings and so on, is performed. The output is quasi-real (simulated) accelerations.

The output of Fig. 4 is the input for Fig. 5 where the accelerometer itself is described. It covers the application of equations (13) and (14). First the input acceleration is integrated twice. Then the negative parasitic stiffness (ω_p^2) and internal and external noise effects are considered. Towards the right side one has still the damping and the integral part which are all combined. After scaling and filtering the frequencies above the measurement bandwidth one obtains the quasi-measured accelerations.

Fig. 6 describes shortly a simple attitude control system. Using angular velocities (denoted here as n) and angles ('Winkel') as input, one can compute torques by an appropriate combination of the scaled input parameters. The division by the moments of inertia $\mathbf{I}$ of the S/C leads to angular accelerations which are the input quantities to fire the thrusters for attitude control.

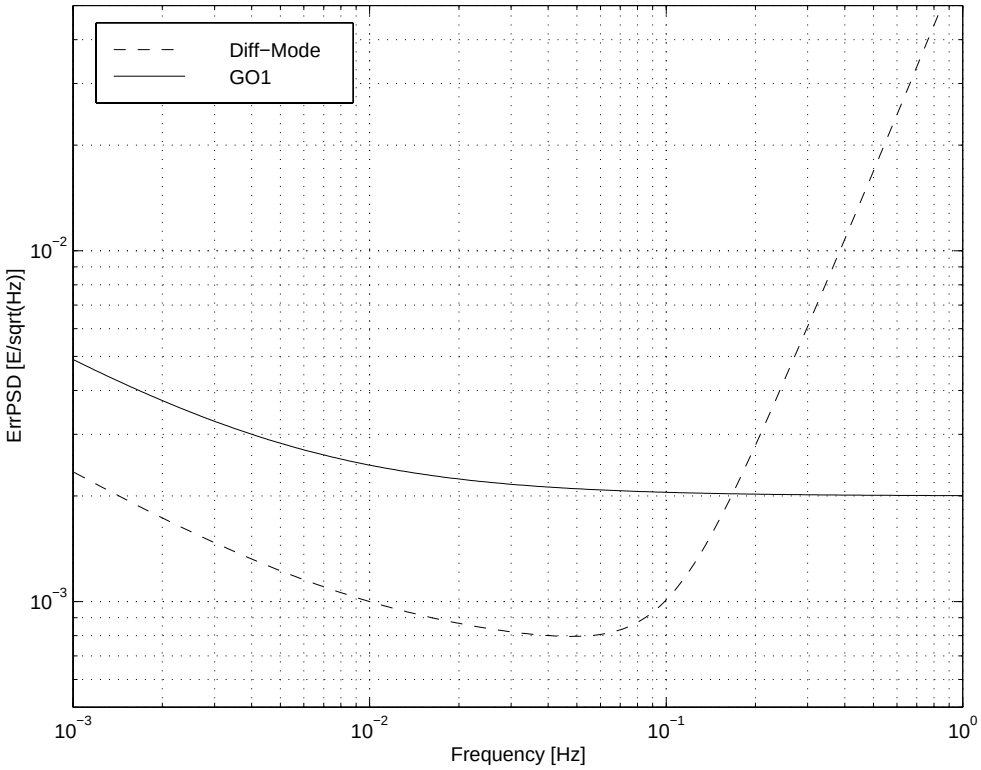

Figure 8: Theoretical noise spectra of the accelerometer measurements.

4 First results

We have tested the DFC part by investigating whether we are able to control the required linear acceleration up to a certain level (10^{-7} m/s$^2/\sqrt{\text{Hz}}$ in the measurement bandwidth). Fig. 7 shows the drag spectra in along-track direction (dotted line) and the PSD of the controlled acceleration in the same direction (solid line). The dashed curve below indicates the expected thruster noise for DFC. It lies below the required accuracy level. Our investigations have further shown that we can perform the linear control at least one order of magnitude better (which is probably required for the capacitive instrument) by tuning the parameters of the corresponding transfer function. This will be discussed in more detail in a follow-on paper.

Furthermore we have tested whether the theoretically expected accuracy of the accelerometer measurements can be reproduced by our simulator. Fig. 8 gives the expected error curve caused by the assumed noise levels (one applied as input acceleration noise, one as internal position sensing noise) already converted to Eötvös units. For comparison the curve GO1 is shown which represents the baseline assumption for the error spectrum of the gradiometer. This curve has been provided by ONERA and is used in the global GOCE simulations as long as one has no better information about the real error behaviour. It served also as upper limit to derive requirements for the mission parameters like e.g. pointing stability or misalignments.

Fig. 9 shows the noise spectra which were obtained by running the whole simulator; the in-line tensor components are plotted simultaneously. The agreement between the noise curve in Fig. 8 and those of Fig. 9 is excellent, also when high-frequent noise is present. Obviously the measurement precision of the accelerometer lies well beyond the aspired level of 10^{-3} Eötvös$/\sqrt{\text{Hz}}$ in the measurement bandwidth.

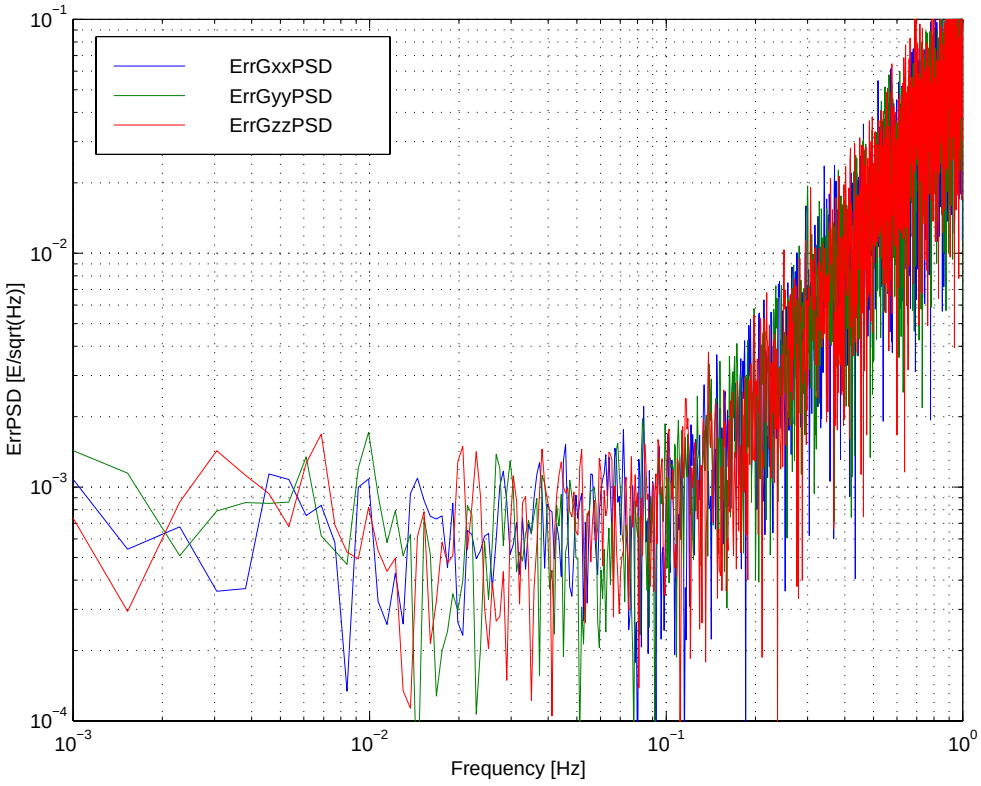

Figure 9: Observed noise spectra with the simulator.

These first tests show that the simulator is a powerful tool for investigating both the gradiometric part of GOCE as a whole and the various subsystems separately.

5 Outlook

Currently the simulator still suffers from some shortcomings related to the software itself. The software runs on a PC which is limited in memory and speed. Therefore a large amount of computer time is needed (a couple of hours for one orbit). A lot of calculations are done by standard tools which are provided in SIMULINK and can not be exchanged easily. For example, we use the given integrators without being able to change their specifications. Thus this part functions as a black box. We are limited in our possibilities to optimise the system in accuracy and speed, but we work on it to make the system more comfortable.
As a consequence of the current status one has to plan very carefully before running some test cases. What can be done is to stabilize the program and to increase its robustness. Also the internal modelling can still be improved (e.g. the right choice of filters for cutting high-frequent noise). In addition more realistic noise scenarios for the simulation of misalignments have to be found.
Up to now, we can test various accelerometer parameters and the effect of perturbing forces like drag or satellite rotations. We can simulate different accuracies for each accelerometer axis and introduce separate misalignments and scale factors for the different directions. We can incorporate an improved DFC (e.g only in the measurement bandwidth or for all frequencies). A next step will be to close the loop for attitude control, i.e. to use our own 'measured' angular velocities for S/C control.

Furthermore we control our simulation results by linear control theory; that means, we extract single parts of the complex mission (e.g. drag-free control or the coupling of misalignments) and compute their effects separately.
In short our simulator is very well able to validate the results of the GOCE simulator running at SRON.

Acknowledgement

We like to thank our colleague Nico Sneeuw for many fruitful discussions and for providing the flow chart showing the division of the tasks within the SID consortium (Fig. 1). We thank Prof. Reiner Rummel for carefully reading the manuscript and a lot of helpful suggestions for improving its understanding. We are very grateful to Martijn Smit from SRON who went critically through the paper for improving the representation of the topic.

References

[1] Hoyng P. (1997). *High Tides for GOCE*, SRON, Docnr. I-G-001SR/97.

[2] Kaplan M. (1976). *Modern Spacecraft Dynamics & Control*, John Wiley & Sons.

[3] Rummel R. (1986). *Satellite Gradiometry*, in: "Mathematical and Numerical Techniques in Physical Geodesy", Lecture Notes in Earth Science **7**, ed. by H. SÜNKEL, Springer, Berlin, 318-363.

[4] Schneider M. (1992). *Himmelsmechanik*, Bd. I, BI Wissenschaftsverlag.